Green Chemistry

PAPER

View Article Online
View Journal | View Issue

Cite this: *Green Chem.*, 2021, **23**, 5656

An efficient approach to synthesizing 2,5-bis(*N*-methyl-aminomethyl)furan from 5-hydroxymethylfurfural *via* 2,5-bis(*N*-methyl-iminomethyl)furan using a two-step reaction in one pot†

Jie Zhang,[a] Wenlong Jia,[a] Yong Sun, *[a,b,c] Shuliang Yang,[a,b] Xing Tang,[a,b] Xianhai Zeng[a,b] and Lu Lin[a,b]

In this study, an amination–oxidation–amination–reduction (AOAR) strategy was proposed for the synthesis of 2,5-bis(*N*-methyl-aminomethyl)furan (BMAF) from HMF *via* the intermediate 2,5-bis(*N*-methyl-iminomethyl)furan (BMIF). Firstly, an efficient synthesis of BMIF from HMF using a one-pot amination–oxidation–amination reaction was developed over α-MnO_2 under an air atmosphere. A BMIF yield of 98.3% was obtained under mild reaction conditions. The conversion of HMF to BMIF underwent the fast amination of HMF to 5-(methyl-iminomethyl)furfuryl alcohol (MIFA), the subsequent rate-limiting oxidation of MIFA to 5-(methyl-iminomethyl)furfural (MIFF) and the final fast amination of MIFF to BMIF. The quick amination of MIFF to BMIF drove the oxidation reaction equilibrium toward MIFF from MIFA, which ensured the highly efficient conversion of HMF to BMIF. The investigation of the catalytic mechanism showed better lattice oxygen donating ability and oxygen coordination capacity, which made α-MnO_2 retain the structural stability in the reaction. The higher ratio and better mobility of the lattice oxygen endowed α-MnO_2 with excellent catalytic performance in the oxidation of MIFA to MIFF by the redox cycling of Mn^{4+}/Mn^{3+}, facilitating the conversion of HMF to BMIF. Eventually, a BMAF yield of 96.1% was achieved by the reduction of BMIF with Ru/C after the AOA reaction, realizing the synthesis of BMAF from HMF using a two-step reaction in one pot.

Received 9th May 2021,
Accepted 24th June 2021

DOI: 10.1039/d1gc01635k

rsc.li/greenchem

Introduction

Diamines are important intermediates in pharmaceuticals, food additives and fine-chemicals. They also act as material monomers for the large-scale production of numerous polymers, including polyamides, epoxy polymers and polyureas, which are increasingly used in health applications and aerospace, automotive, agrochemical and building industries.[1–4] Biomass is one such resource that has attracted significant attention due to its high abundance. With great social concerns about energy and the environment, the catalytic conversion of lignocellulosic biomass to renewable versatile diamines has been extensively researched.[5–7] A prevalent strategy is to convert lignocellulosic biomass to platform chemicals,[8–13] such as 5-hydroxymethylfurfural (HMF), furfural and levulinic acid, in the first step, and then the corresponding diamines can be produced through a series of further reactions.[14–17]

In recent years, some progress has been made in seeking sustainable solutions for the production of furan-diamines from renewable biomass-derived HMF. Several strategies for the preparation of furan-diamines from HMF have been explored, including the stepwise amination pathway, oxidation–amination pathway and amidation–amination pathway, as shown in Scheme 1. For the stepwise amination pathway, HMF is converted to 5-aminomethyl-furfuryl alcohol (AMF) by reductive amination or reduced to 2,5-bis(hydroxymethyl)furan (BHMF), and then AMF or BHMF is directly aminated to furan-diamines *via* the hydrogen-borrowing reaction of a hydroxyl group with an amine source.[18–21] This pathway breaks through the direct amination of the hydroxyl group, however, it

[a]*Xiamen Key Laboratory of Clean and High-valued Utilization for Biomass, College of Energy, Xiamen University, Xiamen, 361102, P. R. China. E-mail: sunyong@xmu.edu.cn*
[b]*Fujian Engineering and Research Center of Clean and High-valued Technologies for Biomass, Xiamen, 361102, P. R. China*
[c]*Hubei Key Laboratory of Pollutant Analysis & Reuse Technology Hubei Normal University, Huangshi, 435002 Hubei, P. R. China*

†Electronic supplementary information (ESI) available: Experimental details, catalyst characterization and tests. See DOI: 10.1039/d1gc01635k

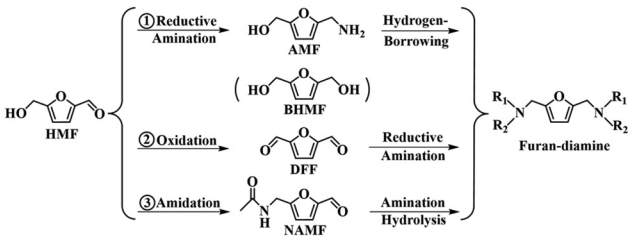

Scheme 1 Renewable synthesis pathway of HMF to furan-diamines.

requires a homogeneous noble metal catalyst to obtain high efficiency. In contrast, prolonging the reaction time and increasing the reaction temperature are necessary for heterogeneous non-noble metal catalysts. Since aldehyde groups facilely react with amines to form furan-amines through reductive amination, 2,5-diformylfuran (DFF) is an ideal starting material to produce furan-diamines. Therefore, the oxidation–amination of HMF is based on the first oxidation of HMF to DFF, and then the reductive amination of DFF.[22–24] Although this reaction route is promising, some problems including an efficient and simple access to produce DFF and the polymerization of furan-amines with DFF by nucleophilic addition, resulting in the drop in the synthesis efficiency of furan-amines, are still needed to be resolved.[25] As for the amidation–amination pathway, furan-amines are generally prepared by the first amidation of the hydroxymethyl group in HMF with CH_3CN using the Ritter reaction, the subsequent amination of the aldehyde group and the final hydrolysis of the acylamino group.[26] This reaction system is relatively complex and the synthesis efficiency is still needed to be enhanced.

In this study, a novel efficient protocol was proposed to synthesize 2,5-bis(*N*-methyl-aminomethyl)furan (BMAF) from HMF using a two-step reaction in one pot. Firstly, HMF was converted to 2,5-bis(*N*-methyl-iminomethyl)furan (BMIF) using the amination–oxidation–amination (AOA) reaction in one pot, followed by the reduction of BMIF to BMAF in the same reaction system. This protocol is characterized by no generation of furan amine-derived polymers that usually occur in the reductive amination of DFF to furan-amines. More specifically, α-MnO_2 showed excellent performance in this system for activating oxygen in air to oxidize HMF with high selectivity. Encouraged by these results, the reaction pathway of HMF to BMIF and the catalytic mechanism were deeply investigated.

Results and discussion

Catalyst screening for the synthesis of 2,5-bis(*N*-methyl-iminomethyl)furan (BMIF)

Building upon our previous work, we found that MnO_2 exhibited excellent performance in the activation of air oxygen to oxidize HMF or 5-[(formate)methyl]furfural (FMF) for the production of maleic anhydride.[27] Moreover, 2,5-diformylfuran was found as a crucial oxidative intermediate in the reaction. Spurred by this, we tried to develop a novel synthesis system that enables the ultraselective production of BMIF by integrating the oxidation and amination of HMF in one pot using air as an oxidant over MnO_2. As is well known to all, MnO_2 has various crystallographic structures, which significantly influence the catalytic property during oxidation.[28,29] At the outset of our work, the investigation was focused on the performance of MnO_2 catalysts with different crystalline phases (including α-, β-, and γ-MnO_2). Excitingly, these three crystalline MnO_2 catalysts exhibited excellent catalytic activity, especially α-MnO_2 gave a better BMIF yield (98.3%) than γ- and β-MnO_2 (Table 1, entries 2–4). In addition, several other transition metal catalysts (such as Fe-, Cu-, Zn-, V-, and Mo-based oxides or salts) usually used for the oxidation of HMF to DFF were also examined in this AOA reaction,[30–34] but all candidates failed to give satisfactory results (Table 1, entries 5–11). It is worth noting that the targeted products, such as MIFA and BMIF, were not found in Table 1, entries 9–11, however, an unknown compound with a relative molecular mass of 237 (denoted as MW237) as the main product was detected by GC-MS measurement (Fig. S1†). In addition, MIFA was also detected in 0.5 h and 1.5 h when used V_2O_5 as a catalyst (Table S1,† entries 1 and 2). Importantly, the nucleophilic reaction between methylamine and HMF in this study was rapidly completed within 10 min (Table 1, entry 1). Therefore, it is speculated that the unknown compound MW237 should be a dimer from MIFA. Specifically, the reaction solution from the catalysis of MnO_2 was light yellow, however, it became brownish red when V_2O_5 was used as a catalyst (Fig. S2†). The darkened colour of the reaction solution (Fig. S2b†) was probably caused by the polymerization of MIFA with its derivatives.

The reaction profiles of the three kinds of MnO_2 in the AOA reaction are shown in Fig. S3a.† It can be seen intuitively that the catalytic performance of these three MnO_2 catalysts always followed the order of α-MnO_2 > γ-MnO_2 > β-MnO_2 in the whole

Table 1 Catalytic conversion of HMF to BMIF over different catalysts[a]

Entry	Catalyst	Conv. (%)	Yield[b] (%) BMIF	MIFA[c]
1[d]	—	100	0	>99
2	α-MnO_2	100	98.3	<1
3	β-MnO_2	100	84.8	13.9
4	γ-MnO_2	100	93.1	5.7
5	α-Fe_2O_3	100	3.7	76.9
6	γ-Fe_2O_3	100	6.9	81.7
7	CuO	100	5.4	41.7
8	ZnO	100	3.9	53.1
9	V_2O_5	100	0	0
10	$VOSO_4$	100	0	0
11	MoO_3	100	0	0
12[e]	α-MnO_2	100	97.5	1.3
13[e]	β-MnO_2	100	42.7	56.1
14[e]	γ-MnO_2	100	67.3	31.6

[a] Reaction conditions: 0.5 mmol HMF (63 mg), 5.0 mL of 30 wt% methylamine methanol solution, 22 mg of catalyst, 1.0 MPa air, 90 °C, 3 h. [b] Other products were derivatives produced by MIFA. [c] MIFA, 5-(methyl-iminomethyl)furfuryl alcohol. [d] No catalyst, 10 min. [e] The recovered catalyst from the first cycle.

reaction period. The turnover frequencies (TOFs) (Fig. S3b†) of these catalysts showed that their catalytic activity followed the above order. More importantly, the reusability of β- and γ-MnO_2 was poor (Table 1, entries 12–14). Thus, α-MnO_2 was selected as the preferred catalyst for the subsequent study. Meanwhile, the catalytic performance of these three crystalline MnO_2 catalysts clearly demonstrated that the crystal structure has a great influence on the conversion of HMF to BMIF.

Reaction pathway of HMF to BMIF

In general, the lone-pair electron on the N atom of amine spontaneously attacks the carbonyl carbocation on aldehyde *via* a nucleophilic addition, followed by dehydration to form an imine. Adding excess amine to the reaction is a common technique to ensure the stable existence of aldimine.[35–37] In this study, HMF was completely converted into 5-(methyl-iminomethyl)furfuryl alcohol (MIFA) within 10 minutes *via* the nucleophilic addition of the aldehyde group with methylamine even without a catalyst at room temperature, characterized by a fast reaction (Fig. 1 and Fig. S4†).[22] By prolonging the reaction time, BMIF was gradually detected accompanied by a drop in the yield of MIFA, as shown in Fig. 1. The product distribution with the reaction course inferred that the conversion of HMF to BMIF certainly underwent a stepwise reaction of HMF to MIFA, followed by MIFA to BMIF. During the reaction, a little 5-(methyl-iminomethyl)furfural (MIFF) (Fig. S5†) was detected, based on the fact that the fast reaction characteristic of the nucleophilic addition between the aldehyde group and methylamine leads to the formation of an aldimine in this reaction, and it is deduced that the oxidation of a hydroxyl group in HMF to aldehyde should be the rate-limiting step. More importantly, the decrease in the amount of MIFA was matched with an increase in the amount of BMIF, inferring the surface reaction control for the oxidation of MIFA to MIFF.

To gain insight into the molecular evolution that was crucial for the conversion of HMF to BMIF, MIFA was used as the starting material in this study. As expected, more than

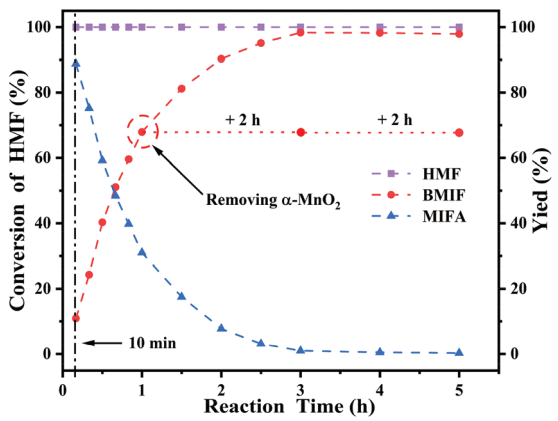

Fig. 1 Time course of the conversion of HMF to BMIF over α-MnO_2. Reaction conditions: 0.5 mmol HMF (63 mg), 5.0 mL of 30 wt% methylamine methanol solution, 22 mg of α-MnO_2, 1.0 MPa air, 90 °C, 3 h.

Table 2 Oxidation reactions of HMF or MIFA under various conditions over α-MnO_2[a]

Entry	Conditions	Conv. (%)	Yield (%) BMIF	DFF	Others[d]	Molar balance
1[b]	40 mmol Methylamine	100	>99	0	—	99
2[b]	—	60.2	23.5	3.9	32.0	99
3	H_2SO_4 (pH = 4, 20 mg) 40 mmol methylamine	100	57.3	0	40.3	98
4	—	37.2	—	22.7	11.7	92
5[c]	—	68.1	—	27.3	37.6	95
6	pH = 6	40.3	—	13.7	25.7	98
7	pH = 4	71.1	—	<1	69.3	97
8	O_2 (1 MPa)	62.5	—	33.1	26.6	96
9	O_2 (1 MPa), pH = 6	43.8	—	8.7	32.8	95
10	O_2 (1 MPa), pH = 4	80.3	—	<1	77.4	96
11	$NaHCO_3$ (20 mg)	78.8	—	48.7	0[e]	62

[a] Reaction conditions: 0.5 mmol HMF, 5.0 mL of MeOH, 22 mg of α-MnO_2, 1.0 MPa air, 90 °C, 3 h. [b] The reaction substrate is 0.5 mmol MIFA. [c] 8 h. [d] Total yields of other products (see the details in Table S2†). [e] GC not detected.

99% BMIF yield was obtained under the investigated conditions (Table 2, entry 1). It has been well recognized that the nucleophilic reaction of an amine and aldehyde to form an aldimine is a reversible reaction. When using MIFA as the starting material without adding methylamine, the 23.5% yield of BMIF and 19.7% yield of HMF suggested the reverse of the reaction equilibrium between HMF and MIFA. More importantly, the 12.3% yield of MIFF and 3.9% yield of DFF further confirmed the oxidation of the hydroxyl group in HMF to the aldehyde group (Scheme 2a, Fig. S6 and S7† and Table 2, entry 2). During this process, methylamine hydrolyzed from MIFA provided the amine source for the formation of BMIF. Therefore, based on the results mentioned above, a reaction pathway for the amination–oxidation–amination of HMF to BMIF is proposed, as illustrated in Scheme 2b. HMF is first rapidly aminated to MIFA, and then the hydroxymethyl group in MIFA is oxidized to an aldehyde group to form MIFF. Subsequently, MIFF continues to quickly aminate to BMIF in the presence of methylamine.

The above results showed that α-MnO_2 exhibited excellent performance in the oxidative amination of HMF to BMIF. Confusingly, by employing α-MnO_2 as a catalyst for the oxidation of HMF in a methanol solution with air, the yield of DFF was less than 23% (Table 2, entry 4). Even when 1 MPa

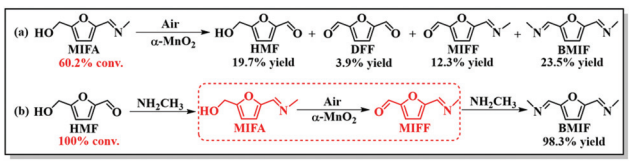

Scheme 2 Oxidation of MIFA (a) and the reaction pathway of AOA from HMF to BMIF (b).

oxygen was used to replace air or the reaction time was prolonged, the yield of DFF was not significantly improved (Table 2, entries 5 and 8). Generally, a relatively acidic environment facilitates the enhancement of the electrophilicity of the carbonyl group, while an alkaline environment favors dehydration to form an imine. Accordingly, the AOA reaction of HMF was conducted in an acidic environment by adding a little H_2SO_4 (Table 2, entry 3), and disappointingly, the yield of BMIF dropped significantly, which was probably due to the instability of the Schiff base (MIFA, MIFF and BMIF) in an acidic environment. Likewise, in an acidic environment, less than 15% DFF was obtained from the oxidation of HMF using air as an oxidant, and almost no DFF was generated under a 1 MPa O_2 atmosphere (Table 2, entries 6, 7, 9 and 10), whereas an alkaline environment clearly favored the oxidation of HMF to DFF when using $NaHCO_3$ as an alkali source (Table 2, entry 11). In summary, an alkaline environment was made for the oxidation of a hydroxyl group to an aldehyde group and MIFA, MIFF and BMIF were formed in this study. More importantly, the amination of MIFF to BMIF characterized by a fast reaction also facilitated the oxidation reaction equilibrium toward MIFF from MIFA, which enhanced the apparent efficiency in the conversion of HMF to BMIF.

Catalytic mechanism of MnO_2 for the conversion of HMF to BMIF

To elucidate the structural characteristics of the synthetic MnO_2, XRD, N_2 adsorption/desorption isotherm, SEM and FT-IR analyses were conducted. Initially, the phase structure of the synthetic MnO_2 was characterized by powder XRD. As shown in Fig. 2a, the XRD patterns were in good agreement with tetragonal α-MnO_2 (JCPDS 44-0141), tetragonal β-MnO_2 (JCPDS 24-0735) and orthorhombic γ-MnO_2 (JCPDS 14-0644), respectively, meaning that these three kinds of MnO_2 were successfully synthesized.[38] The average sizes of fresh α-, β-, and γ-MnO_2 calculated using the Scherrer equation on the basis of the XRD patterns were 22.1, 45.7, and 11.3 nm, respectively. As shown in the FT-IR pattern (Fig. S8†), the band at 3450 cm^{-1} is attributed to the O–H stretching vibration, and the bands at 1630, 1385, 1120, and 1025 cm^{-1} are normally attributed to the O–H bending vibrations combined with Mn atoms. In the fingerprint area, α-, β-, and γ-MnO_2 present different IR spectra with the stretching vibration originating from the Mn–O–Mn and Mn–O bonds in [MnO_6] octahedra.[39–41] Perhaps, the distinct crystalline or morphological characteristics are mainly attributed to the difference in bonding among these three MnO_2 catalysts, ultimately affecting their catalytic performance.

To further figure out the morphology of the catalyst surface, the synthetic MnO_2 was observed by SEM (Fig. S9–S11†). These three MnO_2 catalysts with different crystal phases obviously presented different morphologies, and most of them were less than 1.5 micrometers in length and tens of nanometers in width, with a large aspect ratio, which agreed well with the XRD result. Obviously, α-, β-, and γ-MnO_2 were 1D structural materials, and α-MnO_2 showed a needle-like shape, β-MnO_2

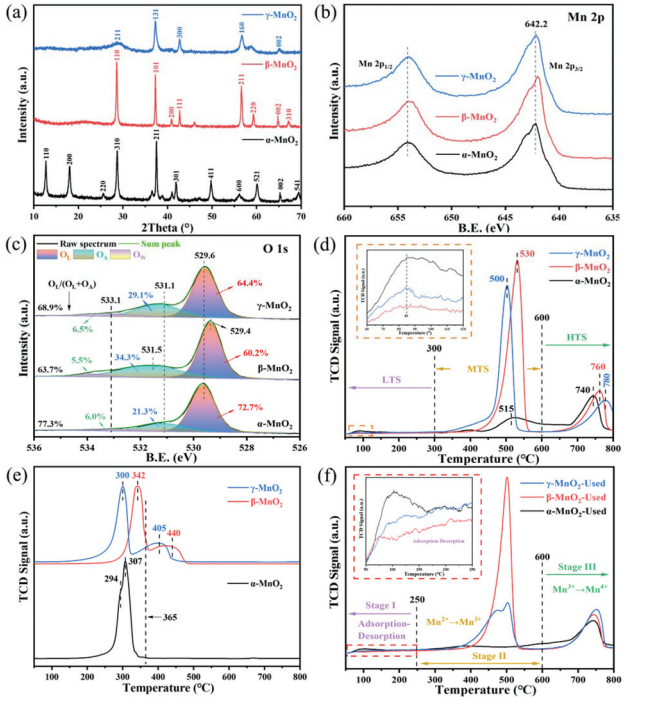

Fig. 2 Characterization analyses of MnO_2: XRD patterns of the fresh α-MnO_2, β-MnO_2, and γ-MnO_2 (a); XPS spectra of Mn 2p (b) and O 1s (c) of MnO_2; O_2-TPD (d) and H_2-TPR (e) of fresh MnO_2; and O_2-TPO (f) of the recovered MnO_2.

presented rod-like nanorods and γ-MnO_2 consisted of straight and radially grown nanorods characterized by urchin-like structures. As shown in Fig. S12†, these three kinds of MnO_2 showed type IV isotherms with a type H1 hysteresis loop, indicating the mesoporous structure of the MnO_2 nanorods.[42] Specifically, Brunauer–Emmett–Teller (BET) characterization by N_2 adsorption/desorption showed that the specific surface area and pore volume of α-MnO_2 were higher than those of β-MnO_2 and γ-MnO_2, corresponding to its slender needle-like structure (Table 3). A larger BET surface area and pore volume, together with a relatively smaller crystal size, imply a larger crystal surface area, which facilitates the shift of oxygen among the surface lattice, absorbed oxygen on the crystal surface and substrate.

To identify the surface species of Mn and O, these three MnO_2 catalysts were examined by XPS measurement. As shown in Fig. 2b and c, the characteristic peaks of Mn $2p_{3/2}$ in α-, β-, and γ-MnO_2 were located at around 642.2 eV, indicating that Mn^{4+} was predominant in these three crystalline MnO_2 cata-

Table 3 Particle morphology, surface area, pore volume, and crystal size of MnO_2 catalysts

Sample	Morphology	BET surface area (m^2 g^{-1})	Pore volume (cm^3 g^{-1})	Crystal size (nm)
α-MnO_2	Needle-like	22.12	0.124	22.1
β-MnO_2	Rod-like	13.06	0.075	45.7
γ-MnO_2	Urchin-like	20.54	0.112	11.3

lysts.[43] The broad O 1s peaks can be deconvoluted into peaks at 529.4–529.6 eV, 530.8–531.5 eV, and 533.1–533.7 eV, corresponding to the lattice oxygen (O^{2-}) (denoted as O_L); the adsorbed oxygen O_2^{2-}/O^-, hydroxyl species and carbonate (CO_3^{2-}) (denoted as O_A); the adsorbed molecular water (denoted as O_W), respectively.[44] The surface oxygen species ratios ($O_L/(O_A + O_L)$) were calculated and are summarized in Table S3,† entries 1–3. Obviously, α-MnO_2 (77.3%) had a higher ratio of $O_L/(O_A + O_L)$ than γ-MnO_2 (68.9%) and β-MnO_2 (63.7%), which was in good accordance with the order of the catalytic activity for the conversion of HMF to BMIF using the AOA reaction.

The mobility of oxygen species in these three MnO_2 catalysts was assessed by O_2-TPD. As shown in Fig. 2d, the O_2-TPD profiles are divided into three stages: Low-Temperature-Stage (LTS) peaks at <300 °C, Medium-Temperature-Stage (MTS) peaks at 300–600 °C and High-Temperature-Stage (HTS) peaks at >600 °C, corresponding to the physically adsorbed oxygen (LTS-oxygen), strong chemically adsorbed oxygen (MTS-oxygen) and its bulk lattice oxygen (HTS-oxygen), respectively.[45,46] For all the MnO_2 samples, the desorption of LTS-oxygen is similar, and three small humps are observed at 85 °C (Fig. 2d inset). Besides, a weak peak at 515 °C and a strong peak at 740 °C were observed for α-MnO_2, while two strong peaks centred at 530 °C and 760 °C for β-MnO_2, and significant peaks at 500 °C and 780 °C for γ-MnO_2 were observed. As is known, LTS- and MTS-oxygen participates in the suprafacial reaction mechanism, while HTS-oxygen is relevant for a Mars-van Krevelen redox cycle.[47] In the O_2-TPD profiles, the intensity of the desorption peaks related to the chemically adsorbed oxygen followed the tendency: β-MnO_2 > γ-MnO_2 ≫ α-MnO_2. Based on the catalytic activities of these three MnO_2 catalysts, obviously, the chemically adsorbed oxygen of MnO_2 is hardly involved in the oxidation of MIFA to MIFF, unlike HTS-oxygen. Curiously, although the discrepancy in the HTS-oxygen desorption temperature was not obvious, the HTS-oxygen desorption temperature was not consistent with the catalytic activity, probably caused by their different structure. The escape velocity of the internal lattice-oxygen probably initially influenced by tunnel sizes of 1 × 2 (2.3 Å × 4.6 Å) in γ-MnO_2, until the collapse of the crystal. While for β-MnO_2 with tunnel sizes of 1 × 1 (2.3 Å × 2.3 Å), owing to the limitation of narrower tunnel sizes, the lattice-oxygen probably mainly desorbed for the crystal plane at the initial desorption stage, resulting in a relatively lower desorption temperature than that of γ-MnO_2. More importantly, the lattice oxygen ratio of MnO_2 (integrated from the curve at MTS and HTS, S_{HTS}/S_{MTS}) intuitively followed the order of the catalytic activity: α-MnO_2 > γ-MnO_2 > β-MnO_2, agreeing with the results of XPS analysis. Accordingly, it is deduced that the lattice oxygen ratio of MnO_2 is a vital factor for the AOA reaction of HMF to BMIF.

H_2-TPR analysis was performed to investigate the relative reducibility of these three MnO_2 catalysts, as shown in Fig. 2e. The green colour after H_2-TPR (see Fig. S13†) indicated that MnO_2 was completely reduced to MnO, the final reduction state. For β-MnO_2, strong and weak reduction peaks of H_2 consumption were observed at 342 and 440 °C. As for γ-MnO_2, strong and weak reduction peaks of H_2 consumption were observed at 300 and 405 °C. The strong and weak reduction peaks represent the reduction of MnO_2 to Mn_3O_4 and the subsequent reduction of Mn_3O_4 to MnO, respectively.[48,49] Obviously, the reducibility of γ-MnO_2 was better than that of β-MnO_2, whereas for α-MnO_2, two peaks of H_2 consumption were observed at 294 °C and 307 °C; the former reduction peak may be attributed to the reduction of MnO_2 to Mn_2O_3 (or Mn_3O_4), and the latter was assigned to the final reduction to MnO. The reduction temperature of α-MnO_2 was obviously lower than those of β-MnO_2 and γ-MnO_2, especially in the reduction stage of Mn_2O_3 or Mn_3O_4 to MnO. As a result, α-MnO_2 possessed the most reducibility. In general, a strong Mn–O bond also limits the mobility of the lattice oxygen. The average bond lengths of Mn–O in α-MnO_2, β-MnO_2 and γ-MnO_2 are 1.98, 1.88, and 1.91 Å, respectively,[43] meaning that the Mn–O bond strength decreases in the order of α-MnO_2 < γ-MnO_2 < β-MnO_2, whereas the reducibility is opposite. Taken together, the oxygen species mobility of the three kinds of MnO_2 is consistent with the order of their catalytic activity, inferring that α-MnO_2 has excellent lattice oxygen donating ability.

Furthermore, O_2-TPO analysis was employed to investigate the oxidability of the recovered MnO_2 after the reaction. As shown in Fig. 2f, O_2-TPO profiles of the recovered MnO_2 are also split into three stages, one below 250 °C is assigned to the adsorption–desorption of O_2 at low temperature. The latter two stages at 250–600 °C and above 600 °C correspond to the oxidation of Mn^{2+} to Mn^{3+} and the subsequent oxidation process ($Mn^{3+}\rightarrow Mn^{4+}$), respectively.[42] The O_2-TPO profiles showed that the reduced state of Mn^{2+} was dominant in the recovered β-MnO_2 and γ-MnO_2, however, the reduced state in the recovered α-MnO_2 was almost in the form of Mn^{3+}, which suggested the redox cycling of Mn^{4+}/Mn^{3+} for α-MnO_2 as a catalyst, and the redox cycling of $Mn^{4+}/Mn^{3+}/Mn^{2+}$ for β-MnO_2 and γ-MnO_2. Obviously, the oxygen consumption required for the recovered MnO_2 followed the rule of β-MnO_2 > γ-MnO_2 ≫ α-MnO_2, meaning that α-MnO_2 had a higher valence after the reaction and a stronger oxygen coordination capacity compared to γ-MnO_2 and β-MnO_2 under an air oxygen atmosphere. To further confirm the valence state of the manganese species during the reaction, the recovered α-, β-, and γ-MnO_2 after the reaction under a N_2 atmosphere (denoted as the used α-, β-, and γ-MnO_2 in N_2) were analysed by XPS. As shown in

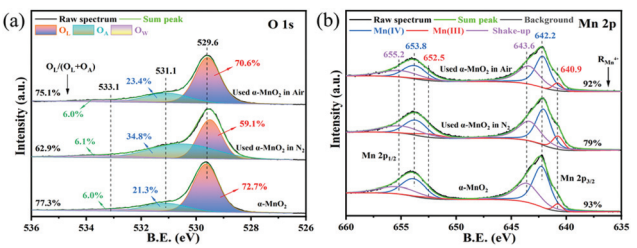

Fig. 3 O 1s (a) and Mn 2p (b) spectra of the fresh and the recovered α-MnO_2 (reaction under a 1.0 MPa N_2- or air-atmosphere).

Fig. S14,† the recovered α-MnO_2 did only contain Mn^{4+} and Mn^{3+}, while a large amount of Mn^{2+} was observed in β-MnO_2 and γ-MnO_2, which further confirmed the above-mentioned result of O_2-TPO analysis.

To evaluate the oxygen coordination capacity of α-MnO_2, the recovered α-MnO_2 (reaction under a 1 MPa N_2- or air-atmosphere, denoted as the used α-MnO_2 in N_2 and the used α-MnO_2 in air) was subjected to XPS analysis. The $O_L/(O_A + O_L)$ ratio of the used α-MnO_2 in N_2 decreased from 77.3% to 62.9%, but that in air only dropped slightly (Fig. 3a). Similarly, the proportion of Mn^{4+}/Mn (denoted as R_{Mn}^{4+}) for the used α-MnO_2 in N_2 was dropped to 79% from 93%, whereas almost no change was observed for the used α-MnO_2 in air (Fig. 3b). Generally, three crystalline MnO_2 catalysts are constructed from the MnO_6 octahedron in different bonding ways, and the dimensions of the channels (2 × 2) (4.6 Å × 4.6 Å) in α-MnO_2 are larger than those in β-MnO_2 (1 × 1, 2.3 Å × 2.3 Å) and γ-MnO_2 (2 × 1, 4.6 Å × 2.3 Å); moreover, the molecule diameter of oxygen is 0.35 nm, which is conducive to the shift of the surface oxygen into the lattice of α-MnO_2.[29] These results demonstrated that the lattice oxygen of α-MnO_2 certainly drove the oxidation of the hydroxyl group to the aldehyde group and was easily recovered under an oxygen atmosphere.

In summary, from the results of XPS, O_2-TPD, H_2-TPR, and O_2-TPO analyses, combining the catalytic performance of these three MnO_2 catalysts, it is reasonably concluded that the lattice oxygen in MnO_2 played a key role in the oxidation of HMF by the redox cycling of Mn^{4+}/Mn^{3+} for α-MnO_2, and the redox cycling of Mn^{4+}/Mn^{3+} and Mn^{3+}/Mn^{2+} for β-MnO_2 and γ-MnO_2; moreover, α-MnO_2 exhibited the better mobility of lattice oxygen.

Based on the results described above, the catalytic pathway for the AOA reaction of HMF over α-MnO_2 was proposed as shown in Scheme 3. Initially, the aldehyde group attached to HMF spontaneously reacts with methylamine to form MIFA. Meanwhile, the hydroxyl group in MIFA is adsorbed on the surface of MnO_2 and subsequently oxidized to the aldehyde group by the lattice oxygen, accompanying the reduction of Mn^{4+} to Mn^{3+}. The resultant MIFF is dissociated from the surface of MnO_2, followed by a further amination to obtain BMIF. Finally, Mn^{3+} is oxidized to Mn^{4+} by the adsorbed oxygen on the surface of the catalyst, resulting in the recovery of MnO_2.

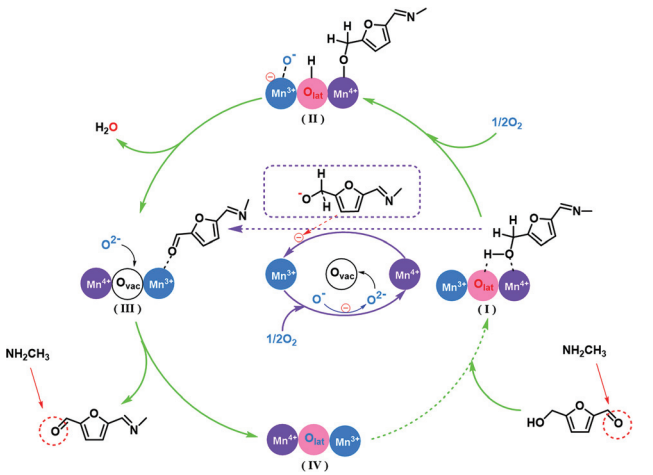

Scheme 3 A plausible mechanistic pathway for the AOA transformation of HMF into BMIF with α-MnO_2 under air (O_{vac} and O_{lat} represent oxygen vacancy and lattice oxygen).

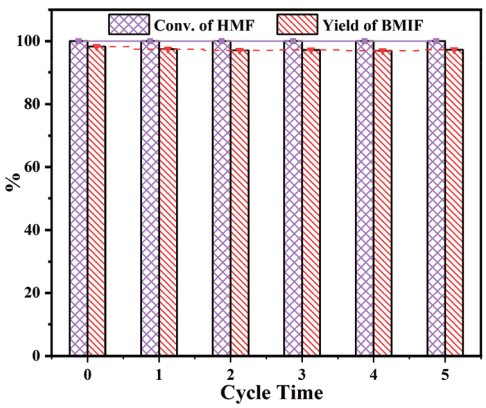

Fig. 4 Recycling tests of α-MnO_2 on the conversion of HMF to BMIF. Reaction conditions: 0.5 mmol HMF (63 mg), 5.0 mL of 30 wt% methylamine methanol solution, 22 mg of fresh or recovered α-MnO_2, 1.0 MPa air, 90 °C, 3 h.

Leaching and reusability tests of α-MnO_2

In order to investigate the stability of these three MnO_2 catalysts in the AOA reaction of HMF to BMIF, the recycling tests of the recovered MnO_2 were conducted. The catalyst was separated from the reaction mixture by filtration after the reaction, and then dried at 60 °C for 2 h before reuse in the next cycle. Excitingly, the catalytic activity of the recovered α-MnO_2 (97.5% yield) still retained a high level (Fig. 4), whereas a significant decrease for the recovered β-MnO_2 (42.7% yield) and γ-MnO_2 (67.3% yield) was observed (Table 1, entries 12–14). Then, the recovered α-MnO_2, β-MnO_2 and γ-MnO_2 after the reactions (Table 1, entries 12–14) were characterized by XRD (Fig. S15†). It was found that only α-MnO_2 still retained its original crystalline structure (Fig. S16a†), and the Mn–O and Mn–O–Mn bonds in the fingerprint area showed hardly any change (Fig. S16b†), even after the fifth cycle, while structural collapse was observed for β-MnO_2 and γ-MnO_2. These results showed that the structural stability of α-MnO_2 also was a crucial factor for its excellent performance in the AOA reaction of HMF to BMIF.

To further investigate the stability of α-MnO_2, the leaching test was carried out after the reaction for 1 h. No further conversion of HMF was observed even prolonging the reaction time to 5 h (Fig. 1), demonstrating that the active species did not leach into the reaction solution.

Reduction of BMIF to BMAF

To realize the synthesis of BMAF from HMF using a two-step reaction in one pot (Scheme 4), several commercial catalysts, such as RANEY®-Ni, RANEY®-Co, Pt/C, Pd/C and Ru/C, were

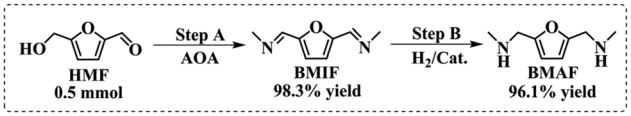

Scheme 4 Synthesis of BMAF from HMF using a two-step reaction in one pot. Reaction conditions: step A, 0.5 mmol HMF (63 mg), 5.0 mL of 30 wt% methylamine methanol solution, 22 mg of α-MnO_2, 1.0 MPa air, 90 °C, 3 h; step B, 5.0 mL of liquid products from step A, 1.0 mL of 30 wt% methylamine methanol solution, 45 mg of Ru/C, 2.0 MPa H_2, 130 °C, 3 h.

Table 4 Catalytic reduction of BMIF over different catalysts[a]

Entry	Catalyst	Time (h)	Conv. (%)	Yield (%)
1	RANEY®-Ni	3	100	64.7
2	RANEY®-Co	3	100	88.7
3	Pt/C (5% Pt)	4	100	12.3
4	Pd/C (5% Pd)	4	100	8.8
5	Ru/C (5% Ru)	3	100	96.1
6[b]	Ru/C	3	100	94.7
7[c]	Ru/C	3	100	95.4

[a] Reaction conditions: 5.0 mL of liquid products from the AOA reaction by α-MnO_2, 1.0 mL of 30 wt% methylamine methanol solution, 45 mg of catalyst, 2.0 MPa H_2, 130 °C. [b] The catalyst was recovered and reused for the 1st run. [c] The catalyst was recovered and reused for the 3rd run.

examined for the reduction of BMIF after the filtration of α-MnO_2 (Table 4, entries 1–5). Owing to the reversible reaction of an aldehyde group and amine to generate an imine, the addition of methylamine is conducive to the stability of imines. Satisfyingly, Ru/C performed well in the reduction of BMIF to BMAF with a yield of 96.1% (Fig. S17†).

To examine the stability of the catalyst, Ru/C was recovered after the reaction for the next run. Encouragingly, no obvious decrease in the catalytic performance for the conversion of BMIF to BMAF was observed after the third cycle (Table 4, entries 6 and 7). In the XRD profiles of Ru/C, no obvious characteristic diffraction peak of Ru was observed for the fresh Ru/C catalyst, indicating good dispersion of Ru. However, the recovered Ru/C catalyst showed a few peaks associated with Ru, which may be caused by the agglomeration of Ru, but the catalytic performance of the recovered Ru/C catalyst was hardly affected (Fig. S18†).

Scope of the AOAR reaction

Finally, several common amines including ammonia, primary amine and secondary amine were examined in the investigated reaction to synthesize other furan-diamines, as shown in Table 5. Almost all amines employed in this reaction obtained a satisfactory yield of the corresponding imine, except ammonia and secondary amine (Table 5, entries 1–8). Owing to the high activity of the primary imine, the imines generated during the reaction of HMF and ammonia easily underwent polymerization to form polymers (Fig. S19a†).[20,25] Generally, the reaction of a secondary amine with a carbonyl group generated the corresponding enamine compound.[36] However, when using HMF as a carbonyl-containing compound, the corresponding enamine was not formed due to no hydrogen at the 2-position of the furan ring (Fig. S19b†). When HMF reacted with a primary amine, owing to no hydrogen at the secondary imine group and 2-position of the furan ring in HMF, the nucleophilic reaction of the aldehyde group with the secondary imine group hardly took place. Therefore, the secondary furan diimine is stable as an intermediate or product in the investigated reaction. So, the protocol to synthesize furan diamines proposed in this study is suitable for secondary furan diamines.

Emphasizedly, it is difficult to efficiently synthesize the furan primary diamines from DFF by direct reductive amination. Recently, Qi *et al.*[23] developed a novel method to synthesize 2,5-bis(aminomethyl)furan from DFF mediated by secondary diimines with the assistance of *trans-imination* with ammonia. Combining the protocol of an efficient synthesis of BMIF from HMF using a one-pot amination–oxidation–amin-

Table 5 Preparation of different furan diimines and diamines[a]

Entry	Substrate	Step A-diimine	$Yield_A$ (%)	Step B-diamine	H_2 (MPa)	Time (h)	Conv. (%)	$Yield_B$[c] (%)
1	Ammonia	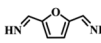	0		—	—	—	—
2		—	0	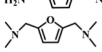	—	—	—	—
3[b]		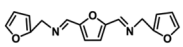	92	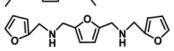	0.3	5	100	87
4		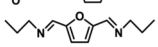	99	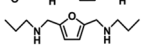	0.5	4	100	97
5		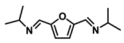	99	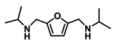	0.5	4	100	96
6			99		0.5	4	100	96
7		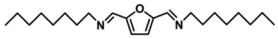	99	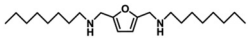	0.5	4	100	98
8[b]		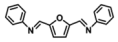	85	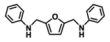	0.2	6	82	53

[a] Reaction conditions: step A: 0.5 mmol HMF, 5.0 mL of 30 wt% substrate methanol solution, 22 mg of α-MnO_2, 1.0 MPa air, 90 °C, 3 h. The conversions were 100%. Step B: 5.0 mL of liquid products from step A, 31 mg of Ru/C, 110 °C. In all reactions, hexadecane was utilized as the internal standard, and the conversions and yields were determined by GC analysis. [b] Step A: 5.0 mL of 10 wt% substrate methanol solution. [c] Furan ring and benzene ring can be reduced.

ation reaction in our study with Qi's study, an alternative strategy for the synthesis of primary furan diamines from HMF by *trans-imination* is promising (Fig. S19c†).

Conclusions

In conclusion, an amination–oxidation–amination–reduction strategy was proposed to synthesize BMAF from HMF *via* the intermediate BMIF using a two-step reaction in one-pot. The crystal structure of MnO_2 had a great effect on the catalytic performance for the oxidation of MIFA to MIFF. Meanwhile α-MnO_2 retained high stability and activity during the reaction. The higher lattice oxygen ratio and better mobility endowed α-MnO_2 with excellent catalytic performance in the oxidation of MIFA to MIFF by the redox cycling of Mn^{4+}/Mn^{3+}, facilitating the conversion of HMF to BMIF, while the redox cycling of Mn^{4+}/Mn^{3+} and Mn^{3+}/Mn^{2+} was required for β-MnO_2 and γ-MnO_2 to finish the oxidation of MIFA to MIFF. Eventually, BMAF was achieved with a yield of 96.1% by the reduction of BMIF over Ru/C under a H_2-atmosphere after the filtration of α-MnO_2, realizing the synthesis of BMAF from HMF using a two-step reaction in one pot. More importantly, the protocol of an efficient synthesis of BMIF from HMF using a one-pot amination–oxidation–amination reaction provides an alternative strategy for the synthesis of primary furan diamines from HMF by *trans-imination*.

Conflicts of interest

There are no conflicts to declare.

Acknowledgements

This work was supported by the National Natural Science Foundation of China (No. 21776234, 21978246) and the research funds from Hubei Key Laboratory of Pollutant Analysis & Reuse Technology (Hubei Normal University).

Notes and references

1 J. M. García, F. C. García, F. Serna and J. L. de la Peña, *Prog. Polym. Sci.*, 2010, **35**, 623–686.
2 H. Zeng and Z. Guan, *J. Am. Chem. Soc.*, 2011, **133**, 1159–1161.
3 A. Corma, S. Iborra and A. Velty, *Chem. Rev.*, 2007, **107**, 2411–2502.
4 C. Moreau, M. N. Belgacemb and A. Gandini, *Top. Catal.*, 2004, **27**, 11–30.
5 K. Murugesan, T. Senthamarai, V. G. Chandrashekhar, K. Natte, P. C. J. Kamer, M. Beller and R. V. Jagadeesh, *Chem. Soc. Rev.*, 2020, **49**, 6273–6328.
6 B. Chen, U. Dingerdissen, J. G. E. Krauter, H. G. J. Lansink Rotgerink, K. Möbus, D. J. Ostgard, P. Panster, T. H. Riermeier, S. Seebald, T. Tacke and H. Trauthwein, *Appl. Catal., A*, 2005, **280**, 17–46.
7 V. Froidevaux, C. Negrell, S. Caillol, J. Pascault and B. Boutevin, *Chem. Rev.*, 2016, **116**, 14181–14224.
8 A. Mittal, H. M. Pilath and D. K. Johnson, *Energy Fuels*, 2020, **34**, 3284–3293.
9 W. Hao, W. Li, X. Tang, X. Zeng, Y. Sun, S. Liu and L. Lin, *Green Chem.*, 2016, **18**, 1080–1088.
10 T. Wang, M. W. Nolte and B. H. Shanks, *Green Chem.*, 2014, **16**, 548–572.
11 X. Kong, Y. Zhu, Z. Fang, J. A. Kozinski, I. S. Butler, L. Xu, H. Song and X. Wei, *Green Chem.*, 2018, **20**, 3657–3682.
12 J. Du, J. Zhang, Y. Sun, W. Jia, Z. Si, H. Gao, X. Tang, X. Zeng, T. Lei, S. Liu and L. Lin, *J. Catal.*, 2018, **368**, 69–78.
13 A. A. Rosatella, S. P. Simeonov, R. F. M. Frade and C. A. M. Afonso, *Green Chem.*, 2011, **13**, 754–793.
14 I. Delidovich, P. J. C. Hausoul, L. Deng, R. Pfützenreuter, M. Rose and R. Palkovits, *Chem. Rev.*, 2016, **116**, 1540–1599.
15 L. T. Mika, E. Cséfalvay and Á. Németh, *Chem. Rev.*, 2018, **118**, 505–613.
16 Y. Xu, X. Jia, J. Ma, J. Gao, F. Xia, X. Li and J. Xu, *Green Chem.*, 2018, **20**, 2697–2701.
17 J. He, L. Chen, S. Liu, K. Song, S. Yang and A. Riisager, *Green Chem.*, 2020, **22**, 6714–6747.
18 D. Pingen, J. B. Schwaderer, J. Walter, J. Wen, G. Murray, D. Vogt and S. Mecking, *ChemCatChem*, 2018, **10**, 3027–3033.
19 K. Zhou, H. Liu, H. Shu, S. Xiao, D. Guo, Y. Liu, Z. Wei and X. Li, *ChemCatChem*, 2019, **11**, 2649–2656.
20 T. Komanoya, T. Kinemura, Y. Kita, K. Kamata and M. Hara, *J. Am. Chem. Soc.*, 2017, **139**, 11493–11499.
21 H. Yuan, B. T. Kusema, Z. Yan, S. Streiff and F. Shi, *RSC Adv.*, 2019, **9**, 38877–38881.
22 J. J. Roylance and K. Choi, *Green Chem.*, 2016, **18**, 5412–5417.
23 H. Qi, F. Liu, L. Zhang, L. Li, Y. Su, J. Yang, R. Hao, A. Wang and T. Zhang, *Green Chem.*, 2020, **22**, 6897–6901.
24 Q. Girka, N. Hausser, B. Estrine, N. Hoffmann, J. Le Bras, S. Marinković and J. Muzart, *Green Chem.*, 2017, **19**, 4074–4079.
25 N. Le, A. Byun, Y. Han, K. Lee and H. Kim, *Green Sustainable Chem.*, 2015, **05**, 115–127.
26 X. Wang, W. Chen, Z. Li, X. Zeng, X. Tang, Y. Sun, T. Lei and L. Lin, *J. Energy Chem.*, 2018, **27**, 209–214.
27 W. Jia, Z. Si, Y. Feng, X. Zhang, X. Zhao, Y. Sun, X. Tang, X. Zeng and L. Lin, *ACS Sustainable Chem. Eng.*, 2020, **8**, 7901–7908.
28 E. Hayashi, Y. Yamaguchi, K. Kamata, N. Tsunoda, Y. Kumagai, F. Oba and M. Hara, *J. Am. Chem. Soc.*, 2019, **141**, 890–900.
29 J. Nie and H. Liu, *J. Catal.*, 2014, **316**, 57–66.
30 F. Bertinchamps, M. Treinen, P. Eloy, A. M. Dos Santos, M. M. Mestdagh and E. M. Gaigneaux, *Appl. Catal., B*, 2007, **70**, 360–369.
31 J. Zhao, A. Jayakumar and J. Lee, *ACS Sustainable Chem. Eng.*, 2018, **6**, 2976–2982.

32 X. Jia, J. Ma, M. Wang, Z. Du, F. Lu, F. Wang and J. Xu, *Appl. Catal., A*, 2014, **482**, 231–236.
33 P. Hu, Y. Chen, X. Yan, W. Lang and Y. Guo, *Ind. Eng. Chem. Res.*, 2019, **58**, 4065–4073.
34 W. Jia, J. Du, H. Liu, Y. Feng, Y. Sun, X. Tang, X. Zeng and L. Lin, *J. Chem. Technol. Biotechnol.*, 2019, **94**, 3832–3838.
35 T. Xiang, X. Liu, P. Yi, M. Guo, Y. Chen, C. Wesdemiotis, J. Xu and Y. Pang, *Polym. Int.*, 2013, **62**, 1517–1523.
36 S. Gomez, J. A. Peters and T. Maschmeyer, *Adv. Synth. Catal.*, 2002, **344**, 1037–1057.
37 W. Chen, Y. Sun, J. Du, Z. Si, X. Tang, X. Zeng, L. Lin, S. Liu and T. Lei, *J. Chem. Technol. Biotechnol.*, 2018, **93**, 3028–3034.
38 B. Zhao, R. Ran, X. Wu and D. Weng, *Appl. Catal., A*, 2016, **514**, 24–34.
39 C. Yuan, L. Hou, L. Yang, D. Li, L. Shen, F. Zhang and X. Zhang, *J. Mater. Chem.*, 2011, **21**, 16035–16041.
40 Y. Xie, Y. Yu, X. Gong, Y. Guo, Y. Guo, Y. Wang and G. Lu, *CrystEngComm*, 2015, **17**, 3005–3014.
41 N. Sui, Y. Duan, X. Jiao and D. Chen, *J. Phys. Chem. C*, 2009, **113**, 8560–8565.
42 F. Gao, X. Tang, H. Yi, C. Chu, N. Li, J. Li and S. Zhao, *Chem. Eng. J.*, 2017, **322**, 525–537.
43 S. Liang, F. Teng, G. Bulgan, R. Zong and Y. Zhu, *J. Phys. Chem. C*, 2008, **112**, 5307–5315.
44 M. Kang, E. D. Park, J. M. Kim and J. E. Yie, *Appl. Catal., A*, 2007, **327**, 261–269.
45 X. Liao, J. Hou, Y. Wang, H. Zhang, Y. Sun, X. Li, S. Tang, K. Kato, M. Yamauchi and Z. Jiang, *Green Chem.*, 2019, **21**, 4194–4203.
46 S. Rong, P. Zhang, F. Liu and Y. Yang, *ACS Catal.*, 2018, **8**, 3435–3446.
47 M. R. Morales, B. P. Barbero and L. E. Cadús, *Fuel*, 2008, **87**, 1177–1186.
48 J. Carnö, M. Ferrandon, E. Björnbom and S. Järås, *Appl. Catal., A*, 1997, **155**, 265–281.
49 R. Xu, X. Wang, D. Wang, K. Zhou and Y. Li, *J. Catal.*, 2006, **237**, 426–430.

